MDPI

Article

Quantum Dielectric Model for Energy Loss of Particles in Astrophysical Plasmas

Claudio D. Archubi [1,*] **and Nestor R. Arista** [2,*]

1 Instituto de Astronomía y Física del Espacio, Universidad de Buenos Aires, Consejo Nacional de Investigaciones Científicas y Técnicas, Ciudad Universitaria, Buenos Aires 1428, Argentina
2 Centro Atómico Bariloche and Instituto Balseiro, Comisión Nacional de Energía Atómica, San Carlos de Bariloche 8400, Argentina
* Correspondence: archubi@iafe.uba.ar (C.D.A.); arista@cab.cnea.ar (N.R.A.)

Abstract: We present the results obtained using a novel quantum approach to describe the interaction of charged particles with the astrophysical type of plasmas, based on the dielectric plasma-wave-packet model (PWPM) together with a full description of statistical effects on energy exchange processes. We use this formulation to calculate the energy loss moments for protons, positrons, and electrons traversing different stellar plasmas on a wide range of projectile velocities and plasma densities and temperatures. We consider special quantum restrictions for the cases of positrons and electrons, including relativistic corrections for high-velocity particles. We analyze and compare the results for different cases of main interest, from dilute solar-corona plasma to cases of increasing densities in the interior of the sun and in the dense regions of giant stars.

Keywords: interactions; particles; stars; plasmas; proton; electron; positron

PACS: 34.50.Bw

1. Introduction

The interaction of subatomic particles with ionized matter at extreme conditions is a subject of great interest for studies in very different areas, including current research on plasma fusion and astrophysical media such as those in stellar interiors [1] or interstellar plasmas [2].

Cosmic rays are fluxes of subatomic particles with high energies that pervade the whole space. They consist mostly of protons and other atomic nuclei produced in the sun and in distant galactic sources, with energies from about 100 MeV to tens of GeV, or velocities from about half to nearly the speed of light. In fact, the complete energy spectrum extends to almost unimaginable high energies of still unknown origin (i.e., particles with energies of up to around 10^{20} eV). Another relevant case is the solar corona, where ions with energies from MeVs to GeVs, and electrons with energies from keVs to about 100 MeVs, are observed.

The cases of astrophysical interest covered by this study span also very wide ranges of plasma conditions, ranging from dilute coronal media in external regions [3,4], to central stellar-core regions where densities may vary from 10^5 to 10^9 g/cm^3, and temperatures rise to values of the order of 10^8–10^9 K as the processes of C, O, Ne, and Si burning in massive stars take place [5–8]. These processes are of outmost importance in the various stages of stellar evolution and in the synthesis of new elements [7,8]. Regions rich in He, C, O, Si, Ne, and other nuclei are predominant in different shells of massive stars in stages that take place before the collapse to the supernova phase [9,10].

In addition, the cases of brown- or red-dwarf stars [11] are also within the general coverage of the present approach, whereas white dwarfs would require a relativistic extension of the description of plasma properties [12,13][1]. Considering the ranges of typical electron speeds in plasmas, the relativistic limits can be estimated at plasma temperatures of ~10^9 K

and electron densities of ~10^{29} cm^{-3} (equivalent to mass densities of ~3×10^5 g/cm^{-3}) for carbon or silicon- rich stars.

With these conditions in mind, the study of interactions between subatomic particles with plasmas at high densities and temperatures become of great interest for the understanding and modeling of energy transport in stellar interiors [1]. In particular, we refer in this study to protons and light particles (electrons and positrons), which show very different features and so are quite appropriate to make a comparative study.

Protons and electrons are the most basic particles participating in stellar processes, starting from primordial hydrogen condensations, while positrons are generated in various nuclear interactions mediated by the weak force (characterized by a continuous spectrum of positron energies associated to neutrino emissions). Thus, for instance in "hot" stars (those in the upper branch of the main sequence, with temperatures over 2×10^7 K) , where the CNO cycle dominates, the most relevant processes that produce energetic positrons (as well as neutrinos, ν_e) are those of N and O decay, namely [7],

$$N^{13} \rightarrow C^{13} + e^+ + \nu_e \tag{1}$$

$$O^{15} \rightarrow N^{15} + e^+ + \nu_e \tag{2}$$

producing positrons with energies that go from very low to MeVs, whereas in "cold" stars (located in the lower side of the main sequence, such as the Sun), the p-p cycle dominates and the main positron sources are

$$p + p \rightarrow d + e^+ + \nu_e \tag{3}$$

and other similar processes involving heavier nuclei.

Therefore, the interest of the present study is to perform a detailed and comparative study of the properties of the main quantities pertaining to the interaction of various charged particles with plasmas in the range of interest for astrophysical applications to stellar media. This includes the calculation of three interaction coefficients: stopping power, energy straggling, and inelastic mean-free path.

Early studies using classical collision models to describe the energy loss of charged particles in plasmas were made by Gryzinski [14], Spitzer [15], and others [16,17]. Additionally, studies using dielectric-function models for classical plasmas have also been made [18–20]. These models, however, cannot be applied in a consistent way to cases where quantum aspects are important, as, for instance, in the cases of electrons or positrons. In the case of ions, classical dielectric models may be used in calculations of stopping powers but require the introduction of quantum cut-offs in the energy loss integrals to avoid divergencies [20]. Furthermore, calculations of other energy-loss moments, such as mean-free paths or energy straggling, require a correct quantum-mechanical approach that escapes the possibilities of classical models. A general theoretical approach that provides a consistent description of the interaction between charged particles and plasma media was introduced in previous works [21,22]. The method contains two basic blocks:

(i) A general statistical description of quantum excitations in a dispersive medium in thermal equilibrium. This is achived by a more general formulation that takes into account the existence of internal excitations in the plasma, described in terms of Bose functions, which allows processes of energy gain and loss in the interaction of external particles with the plasma [23,24].

(ii) A dielectric model for a free electron plasma (or free electron gas, FEG). In the present study, we will make use of the so-called "wave packed model", earlier proposed by Kaneko for atomic systems [25–27], which was more recently adapted to the case of Maxwellian plasmas with Gaussian distributions of electron speeds [22]. This new approach is called the "plasma wave-packet model" (PWPM). The model is based on a full quantum mechanical description of the energy-momentum exchange, which eliminates the need of to introduce a quantum cut-off in the integrals to represent the maximum momentum

transfer, as is required by the classical dielectric-function approach [20]; in the wave-packet model, these properties are implicitly included in the dielectric function, which provides a full quantum treatment of the interactions [21,22].

This work is organized as follows: in Sections 2 and 3, we summarize the theoretical approach and the formulation required for the calculation of energy-loss moments of the various particles. A brief description of the quantum dielectric function for high-temperature plasmas is made in Section 4. In Section 5, we present sample applications of the present approach to different stellar environments, and we discuss in detail the differences found in the results for the various moments and for the three types of particles included in this study. Section 6 contains a summary and the conclusions of this study. Finally, we include three appendices: Appendix A contains a description of the relativistic corrections required for the cases of high-energy particles; Appendix B contains an analysis of the two different contributions to the energy loss moments; and Appendix C contains useful approximations to describe the high and low-velocity limits.

2. General Formulation

A comprehensive quantum-mechanical formulation of the interactions between an external particle with charge Ze and a plasma with temperature T, whose properties are described in terms of its dielectric function $\varepsilon(q, \omega)$, can be made starting from the interaction probability $W(\overrightarrow{q}, \omega)$ given by [23,24]

$$W(\overrightarrow{q}, \omega) = \frac{8\pi(Ze)^2}{\hbar q^2} N(\omega) Im\left[\frac{-1}{\varepsilon(q, \omega)}\right] \tag{4}$$

$W(\overrightarrow{q}, \omega)$ represents the inelastic scattering probability per unit time in an elementary interaction process with momentum transfer $\hbar \overrightarrow{q} = \overrightarrow{p'} - \overrightarrow{p}$ and energy transfer $\hbar\omega = E_{p'} - E_p$, where $\overrightarrow{p}$ and $\overrightarrow{p'}$ are the momenta of the particle before and after the interaction, and E_p and $E_{p'}$ are the corresponding energies. Here, in contrast to the case of zero temperature, both positive and negative frequency values are possible. Processes with $\omega < 0$ correspond to *energy loss processes* by the particle ($E_{p'} < E_p$), while those with $\omega > 0$ correspond to *gain processes*. (Here, loss and gain processes are defined with respect to the external particle, being complementary of corresponding gain and loss processes by the plasma).

In this equation, the factor $N(\omega)$ is the Bose function

$$N(\omega) = \frac{1}{e^{\hbar\omega/k_B T} - 1} \tag{5}$$

where k_B is Boltzmann's constant. This factor represents the thermal distribution of excitations in the plasma and plays the most important role in a full treatment of interaction processes in systems in thermal equilibrium. It carries the information on the existence of thermally activated excitations in the medium, and its presence is crucial to obtain a correct statistical balance between processes of energy exchange (gain and loss processes) between the external particle and the plasma [23,24]. This makes an important difference with respect to previous classical formulations of energy loss effects and will be particularly important in treating the interaction of light particles (like positrons or electrons) with classical or quantum plasmas, as well in calculating energy-loss moments of heavy particles.

The term $Im[-1/\varepsilon(k, \omega)]$ in Equation (4), called the energy loss function (ELF), carries the information on the screening and absorption properties of the plasma (equivalent to the oscillator strength distribution in the treatment of atomic excitations [28]).

Following this approach, we calculate the mean values of the *n*-order moments of the energy loss $\hbar\omega$ given by

$$\frac{d\overline{E}^{(n)}}{dt} = \int \frac{d^3q}{(2\pi\hbar)^3} (\hbar\omega)^n W(\overrightarrow{q}, \omega) \tag{6}$$

And we define the *energy-loss moments* $Q^{(n)}$ (ELM) as

$$Q^{(n)} = \frac{1}{v}\frac{d\overline{E}^{(n)}}{dt} = \frac{(Ze)^2}{\hbar v\pi^2}\int\frac{d^3q}{q^2}(\hbar\omega)^n N(\omega)Im\left[\frac{-1}{\varepsilon(q,\omega)}\right] \tag{7}$$

To perform the integrations appropriately, we consider the relation between the energy and momentum transfers $\hbar\omega$ and $\hbar\overrightarrow{q}$, namely

$$\hbar\omega = E_{p'} - E_p = \frac{1}{2m_p}\left[(\overrightarrow{p} + \hbar\overrightarrow{q})^2 - p^2\right] \tag{8}$$

which yields

$$\omega = \overrightarrow{q}.\overrightarrow{v} + \frac{\hbar q^2}{2m_p} \tag{9}$$

where m_p is the mass of the incident particle and $\overrightarrow{v} = \overrightarrow{p}/m_p$ its velocity before the interaction.

Following this, the expression for the energy-loss moments $Q^{(n)}$ is written as

$$Q^{(n)} = \frac{2}{\hbar\pi}\left(\frac{Ze}{v}\right)^2\int_0^\infty\frac{dq}{q}\int_{\omega_{\min}(q,v)}^{\omega_{\max}(q,v)}(\hbar\omega)^n N(\omega)Im\left[\frac{-1}{\varepsilon(q,\omega)}\right]d\omega \tag{10}$$

with

$$\omega_{\min}(q,v) = -qv + \alpha q^2 \tag{11}$$

and

$$\omega_{\max}(q,v) = qv + \alpha q^2 \tag{12}$$

where $\alpha = \hbar/2m_p$, and m_p is the projectile mass.

The physical meanings of these energy-loss moments, for the cases $n = 0$, 1, and 2, are as follows:

(a) Inverse mean free path:

$$\frac{1}{\lambda} = Q^{(0)} = \frac{2}{\hbar\pi}\left(\frac{Ze}{v}\right)^2\int_0^\infty\frac{dq}{q}\int_{\omega_{\min}(q,v)}^{\omega_{\max}(q,v)} N(\omega)Im\left[\frac{-1}{\varepsilon(q,\omega)}\right]d\omega \tag{13}$$

(b) Stopping power:

$$S = -Q^{(1)} = -\frac{2}{\pi}\left(\frac{Ze}{v}\right)^2\int_0^\infty\frac{dq}{q}\int_{\omega_{\min}(q,v)}^{\omega_{\max}(q,v)}\omega N(\omega)Im\left[\frac{-1}{\varepsilon(q,\omega)}\right]d\omega \tag{14}$$

(c) Energy straggling:

$$\Omega^2 = Q^{(2)} = \frac{2\hbar}{\pi}\left(\frac{Ze}{v}\right)^2\int_0^\infty\frac{dq}{q}\int_{\omega_{\min}(q,v)}^{\omega_{\max}(q,v)}\omega^2 N(\omega)Im\left[\frac{-1}{\varepsilon(q,\omega)}\right]d\omega \tag{15}$$

The minus sign in the stopping power expression agrees with the usual definition $S = -dE/dx$.

Equations (13)–(15) apply straightforwardly to protons and positrons (or other charged particles different from electrons). In the case of electrons, additional restrictions arising from particle identity must be applied; these restrictions will be described below.

In the present formulation, these integrals are calculated with the PWPM procedure mentioned in the Introduction and described in [22]. A fundamental difference between this formulation and the more usual dielectric approach is that the PWPM is a full size quantum formulation that takes into account all the statistical features of the interactions, including gain and loss processes, as well as the quantum restrictions on the possible energy transfers

for incident positrons and electrons. As noted before, in the standard representation of the energy loss process, only positive frequencies are considered [18,20,29–31], whereas in the PWPM method the range of frequencies spans the whole range of negative and positive frequency values (from $-\infty$ to $+\infty$), where the range of negative (positive) ω values represents energy loss (gain) processes by the incident particles.

A detailed explanation of the regions of integration in the $q - \omega$ plane was given in Ref. [22] (*cf.*, in particular, Figure 2 of this reference for a detailed illustration of the integration regions). In the next section, we briefly describe this formulation.

3. PWPM: Individual and Collective Excitations

The integrations specified above cover an open area in the $q - \omega$ plane, with $q > 0$. The response of plasma electrons to the projectile perturbation includes two types of excitations within this area: collective and individual (or binary collisional excitations) [29–32]. The latter represents the most important part of the energy loss for large momentum transfers q, while the collective type of excitation dominates the energy absorption for low-q values [33]. In the case of solids or highly degenerate systems, the collective excitations assume the characteristics of *quasi-particles* (plasmons) with quantized energy values $\sim\hbar\omega_p$, with ω_p being the plasma frequency. Further differences between these two types of excitations are the following: the region of low q and ω values is characterized by strong screening effects and is fairly well described by classical dielectric models; by contrast, for large values of q and ω, the screening weakens and at the same time the quantum properties become most relevant. The main locus of the binary excitations concentrates around the line $\omega_p \sim \hbar q^2/2m$; this is the so-called *Bethe-ridge* and corresponds to hard excitations, with relatively large energy transfers, which may be assimilated to close collisions [28].

It is important to notice that these features of quantum nature are not contained in the classical dielectric-function models [34,35], and for this reason the integrals of the energy-loss moments present divergent behavior when q goes to infinity. This problem is usually circumvented by introducing a cut-off value in the q integrals in a heuristic way [20]. In the present approach, the quantum properties are fully incorporated [32], and this provides regular behavior of the integrals, free of divergencies, so that authomatical convergence is obtained without the need to introduce ad hoc limits.

For the sake of generality, the previous formulas were written in general units; in the following, with m and e being the electron mass and charge, the system of atomic units will be used (i.e., $\hbar = e = m = 1$) unless explicitly stated.

3.1. Individual Excitations

As demonstrated in [22], the energy loss of a particle with charge Z in a plasma with temperature T can be expressed in a unified way in the form

$$Q_{ind}^{(n)} = \frac{2}{\pi}\frac{Z^2}{v^2} \left[\int_{q_c}^{q_{\max}} F_{loss}^{(n)}(q)\, g_x(q)\frac{dq}{q} + \int_{q_c}^{\infty} F_{gain}^{(n)}(q)\, g_x(q)\frac{dq}{q} \right] \tag{16}$$

where the subscript *ind* indicates that only the individual type of excitations are included here. The two terms in Equation (16) represent the energy gain ($\omega > 0$) and energy loss ($\omega < 0$) contributions explained in detail in Ref. [22]. The factor $g_x(q)$ is required in the case of incident electrons because it incorporates the exchange symmetry as a part of the identity effect in the electron–electron interaction. An analytical approximation for this term was obtained by Ochkur for high velocities [36,37][2] and has been largely used in inelastic electron scattering in various media since then [38–40]. Detailed studies made by Hippler [41] and Shinotsuka et al. [42] show that the Ochkur factor considerably improves electron impact ionization and stopping power calculations. Here, we write the Ochkur expression in terms of a relative velocity $v' = (v^2 + v_T^2)^{1/2}$ where $v_T = (3k_BT)^{1/2}$; thus, we have [36][2]:

$$g_x(q) = 1 + (q/v')^4 - (q/v')^2 \tag{17}$$

This factor applies only to the case of electron impact, while $g_x(q) = 1$ for protons and positrons.

The *F*-functions in Equation (16) are given by

$$F_{loss}^{(n)}(q) = \int_{\omega_{\min}}^{0} \omega^n N(\omega) \, G^{(1)}(\omega) \, Im\left[\frac{-1}{\varepsilon(q,\omega)}\right] d\omega \tag{18}$$

and

$$F_{gain}^{(n)}(q) = \int_{\widetilde{\omega}_{\min}}^{\omega_{\max}} \omega^n N(\omega) \, G^{(2)}(\omega) \, Im\left[\frac{-1}{\varepsilon(q,\omega)}\right] d\omega \tag{19}$$

where $\varepsilon(q,\omega)$ is the temperature-dependent dielectric function for an electron plasma in thermal equilibrium, whose properties will be described in the next section.

The functions $G^{(1)}(\omega)$ and $G^{(2)}(\omega)$ in Equations (18) and (19) introduce the quantum restrictions in the electron–electron interactions; this has two aspects: (i) the Pauli exclusion principle and (ii) additional considerations for the energy transfer between identical particles. The first restriction states that the incident electron cannot fall into an occupied state in the plasma. The second one is more particular: it is based on the criterion that, after an electron–electron interaction, the electron that ends up with the largest energy should be considered as the new "primary electron" [43]. This sets a limit to the maximum possible energy transfer. For instance, if E_1 and E_2 are the energies of the incident and target electrons then the maximum energy loss would be $(E_1 - E_2)/2$ (corresponding to the case where both electron have equal energies after the interaction). This value of maximum energy transfer is complementary to the one prescribed by Equation (12), which is common to electrons and positrons. The application of this criterion requires an average over the thermal distribution of energies E_2.

These restrictions apply only to incident electrons and are described in detail in Ref. [22]. For other types of particles, those restrictions disappear, i.e., $G^{(1)}(\omega) = G^{(2)}(\omega) = 1$.

The limits of integration in Equations (18) and (19) are given by Equations (11) and (12). Additionally, in Equation (19) we have introduced a lower limit $\widetilde{\omega}_{\min}$ given by

$$\widetilde{\omega}_{\min}(q,v) = \begin{cases} 0, & q < q_{max} \\ \omega_{\min}(q,v), & q > q_{max} \end{cases} \tag{20}$$

It is clear that for heavy projectiles, $q_{max} \sim \infty$ and $\widetilde{\omega}_{\min} = 0$. Further and detailed information about the different values for the extremes of the q and ω integrals may be found in Ref. [22].

3.2. Collective Excitations

The energy loss due to collective excitations of the FEG was approximated as follows: first, we isolate the contribution of the plasma resonance to the ELF [44] as

$$Im\left[\frac{-1}{\varepsilon(q,\omega)}\right] = \frac{\pi}{D(q)}\left[\delta(\omega - \omega_q) - \delta(\omega + \omega_q)\right] \tag{21}$$

with

$$D(q) = \left|\frac{\partial \varepsilon_1(q,\omega)}{\partial \omega}\right|_{\omega = \omega_q} \tag{22}$$

where ε_1 denotes the real part of ε ($\varepsilon = \varepsilon_1 + i\varepsilon_2$) and ω_q represents the frequency values along the resonance line.

Introducing Equation (21) in the energy loss integrals of Equation (10), we obtain

$$Q_{pl}^{(n)} = 2\frac{Z^2}{v^2}\left[(-1)^{n+1}\int_{q_{\min}^{(1)}}^{q_c}\frac{dq}{q}\frac{(\omega_q)^n}{D(q)}N(-\omega_q) + \int_{q_{\min}^{(2)}}^{q_c}\frac{dq}{q}\frac{(\omega_q)^n}{D(q)}N(\omega_q)\right]$$

$$\tag{23}$$

where q_{min} has two values (for the positive and negative energy zones) according to the explanations given in Ref. [22].

4. Dielectric Function

A general expression for the dielectric function for the case of plasmas in thermal equilibrium, which contains the quantum-mechanical properties of the plasma electrons, is given by [32]

$$\epsilon(q,\omega) = 1 + \frac{e^2}{\pi^2 q^2} \int d^3q' \frac{f(\overrightarrow{q} + \overrightarrow{q'}) - f(\overrightarrow{q'})}{\hbar\omega + i\delta - (E_{\overrightarrow{q}+\overrightarrow{q'}} - E_{\overrightarrow{q'}})} \tag{24}$$

where $E_{\overrightarrow{q}} = \hbar^2 q^2/2m$ and $f(\overrightarrow{q})$ is the Fermi–Dirac distribution function for plasmas of an arbitrary degree of degeneracy,

$$f(\overrightarrow{q}) = \{1 + \exp[\beta(E_q - \mu)]\}^{-1} \tag{25}$$

where $\beta = 1/k_B T$, $E_q = \hbar^2 q^2/2m$, and μ are the chemical potentials of the plasma with electron density n and temperature T. The chemical potential may be calculated with the Fermi–Dirac integral of order $1/2$ using Equation (6) of Ref. [32].

In the limit of high temperatures ($k_B T >> E_F$, with E_F being the Fermi energy of the FEG), where the restrictions imposed by the Pauli principle may be neglected, the imaginary part of ε, denoted $\varepsilon_2(q,\omega)$, takes the Gaussian form [32]

$$\varepsilon_2(q,\omega) \cong \frac{\pi\chi_0^2}{8z^3} \theta\, e^\eta \left[e^{-D(u-z)^2} - e^{-D(u+z)^2} \right] \tag{26}$$

where $u = \omega/qv_F$, $z = q/2k_F$, $\chi_0^2 = e^2/\pi\hbar v_F$, and the factor e^η is approximated in this limit by

$$e^\eta \cong \frac{4}{3\sqrt{\pi}} \frac{1}{\theta^{3/2}} \tag{27}$$

In these expressions, $\theta = k_B T/E_F$ and $D = 1/\theta$, where k_F is the wave vector associated with the Fermi energy E_F.

The variables u and z are those of the Lindhard theory for a degenerate electron gas [29,30]. Using the more appropriate variables $u' = \sqrt{D}u = u/\theta^{1/2}$ and $z' = \sqrt{D}z = z/\theta^{1/2}$ now for the case $k_B T >> E_F$, we may write:

$$\epsilon_2(q,\omega) = \frac{\pi\chi^2}{8} \frac{1}{z'^3} \left[e^{-(u'-z')^2} - e^{-(u'-z')^2} \right] \tag{28}$$

where the parameter χ^2 is given by [21]

$$\chi^2 = \frac{4}{3\sqrt{\pi}} \frac{\chi_0^2}{\theta^2} = \frac{4}{3\sqrt{\pi}} \frac{1}{\pi k_F a_0} \frac{1}{\theta^2} \tag{29}$$

The real part of the dielectric function may be obtained from $\varepsilon_2(q,\omega)$ using the Kramers-Kronig relations; this yields [21]

$$\epsilon_1(q,\omega) = 1 + \frac{\chi^2}{8} \frac{1}{z'^3} \left[W(u'+z') - ZWu' - z') \right] \tag{30}$$

A detailed analysis of the dielectric formulation for the case of Gaussian velocity distributions was made by Kaneko [25–27] and more recently adapted to the case of Maxwellian plasmas in Ref. [22]. A useful expression for the function $W(x)$ obtained from these formulations is the following:

$$W(x) = 2\sqrt{\pi}x \int_0^1 e^{(t^2-1)x^2} dt \tag{31}$$

Related integral forms and further useful approximations for the dielectric function of quantum plasmas are given in Ref. [32].

The key quantity for the calculation of the energy-loss moments is the energy-loss function (ELF), defined by $Im[-1/\varepsilon(q,\omega)] = \varepsilon_2(q,\omega)/[\varepsilon_1(q,\omega)^2 + \varepsilon_2(q,\omega)^2]$.

As demonstrated before [21,22], the present formulation is able to describe the properties of plasmas on a very wide range of densities and temperatures. This approach yields the correct behavior for high temperatures, such that $k_B T >> E_F$, where the use of Gaussian distributions for the electron speeds is quite appropriate. Moreover, an extension of this model to cover the complete range of temperatures, including low ($k_B T << E_F$) and high ($k_B T >> E_F$) limits, as well as the transition range where $k_B T \sim E_F$, can be made by considering an effective temperature T_{eff} obtained by a quadratic interpolation between $k_B T$ and E_F in the form [21]

$$k_B T_{eff} = \sqrt{(k_B T)^2 + \lambda E_F^2} \tag{32}$$

where λ is a fitting parameter. The parameter θ in Equations (15) and (16) is now redefined as $\theta = k_B T_{eff}/E_F$. After a comprehensive set of comparisons [21], we found that the value $\lambda = 0.4$ allows for a very satisfactory representation, on the whole range of temperatures, of the exact results obtained in Ref. [32].

The previous description summarizes the PWPM formulation that will be applied in this work.

5. Calculations for Different Stellar Environments

5.1. Solar Cases

5.1.1. Solar Corona

The solar corona is a complex and not yet well understood dynamical region, composed basically of hydrogen and helium, and small amounts of other elements such as Fe, Si, C, N, and O [45]. Elements such as Fe are relevant to estimate plasma temperatures and densities by spectroscopic analysis. However, since the presence of heavy elements in the solar corona is too small, the contribution of inner shells [46,47] of those elements may be neglected in the present study. The typical values of electron densities and temperatures for the corona region are in the range of 10^8 electrons per cm^3 ($r_s = 2.53 \times 10^5$) and ~10^6 K respectively [45,48,49].

Because of these special conditions, we find it appropriate to start our set of calculations with this system. Hence, in Figure 1 we show the results for the energy loss moments of the different projectiles traversing a plasma region characterized by typical values of density and temperature in the solar corona. The thin red lines in this figure are the analytical approximations for low and high velocities contained in Appendix C. The calculated values show excellent agreement with both approximations.

However, the low density and the high temperature produce significant differences with respect to cold solid-state target densities [21] as well as with values for the solar interior to be shown in the next figure. These differences consist of a decrease in the stopping values, by many orders of magnitude, and a shift of the stopping maximum to higher velocities. The very-low-density values produce also a pronounced decrease in the straggling for all velocities, and a large increase in the mean-free path values.

On the other hand, positrons and electrons demonstrate distinct behaviors. First, we notice the decrease in the stopping power and the straggling values from protons to positrons and electrons; this decreasing behavior is due to quantum restrictions for electrons, and to differences in the maximum energy transfer, which is smaller for light particles than for protons of equal velocities. At high v, the stopping values for protons and light projectiles seem to converge to the same result due to the fact that only a factor inside the logarithmic Bethe limit (see Appendix C) is responsible for the difference. The results for the straggling also show several interesting and new features. The straggling values at high energies show distinct behavior from those of the stopping: this is a consequence of the greater influence of close collisions in the straggling. More precisely, at high velocities the energy straggling is dominated by close collisions (i.e., greater values of momentum

transfers q), and therefore the recoil effect on the value of ω_{min}, given by Equation (11), which is important for light particles, produces a reduction in the maximum momentum transfer in the range of negative frequencies (energy loss terms).
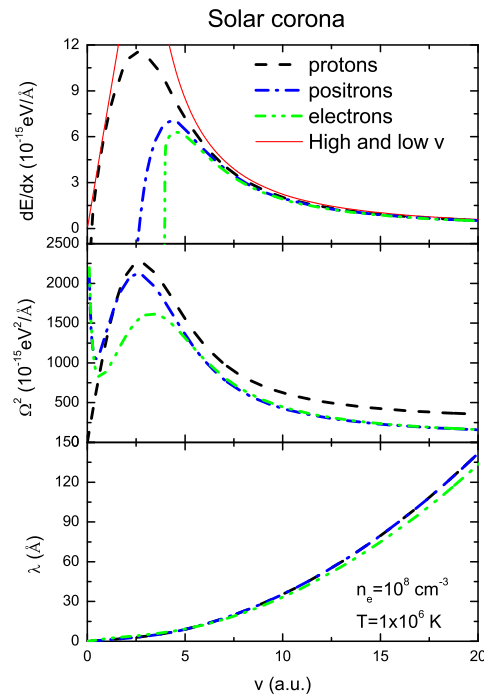

Figure 1. Energy loss moments of protons, positrons, and electrons traversing a solar corona electronic plasma.

Secondly, we notice the anomalous behavior for the cases of electrons and positrons, observed at low velocities, consisting of negative values of the energy loss, and a divergent type of behavior for the straggling. It may be shown that a similar divergency occurs for the inverse-mean-free path (IMFP), although this is not appreciated here because this figure shows the MFP. (The divergent behavior of the IMFP is shown and analyzed in Appendix B). Also, similar effects for protons cannot be observed in this figure because they occur at much smaller velocities. These effects have been analyzed in detail in a previous work [22] and are a direct consequence of the contributions of gain and loss processes, resulting from quantum statistical properties contained in the Bose distribution of thermal excitations.

The effects of thermal fluctuations in the energy exchanges associated with those processes become of increasing importance in the range of sub-thermal energies ($E < (3/2)k_BT$), where the particles can receive energy from the plasma, leading, on average, to negative energy losses [22]. In this region, the image of well-defined particle trajectories is lost, as is the ideal concept of stopping power of light particles with small velocities moving along straight trajectories (the image here is that of a slow particle receiving "kicks" coming from all directions, and so losing the information of the original direction of motion, resulting in a kind of brownian motion). In this case, a more appropriate magnitude to characterize the slowing down process is the mean energy loss/gain per unit time, $d\overline{E}/dt = v d\overline{E}/dx$. It may be shown that in the limit $v = 0$, this quantity, $d\overline{E}/dt$, has a well-defined negative-limit value for the rate of energy loss of electrons and positrons. Similarly, finite but positive values at $v = 0$ can be obtained for the average collision time $\tau = \Lambda/v$ and for the energy straggling per unit time $v\Omega^2 = \langle \Delta E^2 \rangle / \Delta t$. (This means that the divergent behaviors of these quantities, observed in this and the following figures, are of the form $1/v$).

The differences in the mean free path for protons and light particles are very small. The physical interpretation is that the restrictions are relevant for higher energy transfers, which usually correspond to close collisions. Hence, these restrictions produce significant

differences in the straggling, which is dominated by close collisions, but not in the mean free path, which is dominated by distant collisions.

Finally, as the range of velocities considered here runs up to 20 a.u. no relativistic effects are involved.

5.1.2. Solar Interior

We consider now the conditions in the region of the Sun's core, characterized by temperatures and densities of about 16×10^6 K and 160 g/cm^3, respectively and consisting of nearly 75% of hydrogen and 25% of helium. At those temperatures, all the atoms are considered fully ionized. This yields a total electron density of 8.4×10^{25} cm^{-3} ($r_s = 0.268$).

Figure 2 shows the results for the different projectiles traversing a plasma characterized by those values of density and temperature. A more extended range of relativistic velocities is considered here, and a pronounced relativistic rise in the straggling is found. A brief description of the relativistic corrections included in these calculations is given in the Appendix A. The low-velocity and high-velocity limits are in excellent agreement with the corresponding theoretical approximations (described in Appendix C) shown by the red lines.
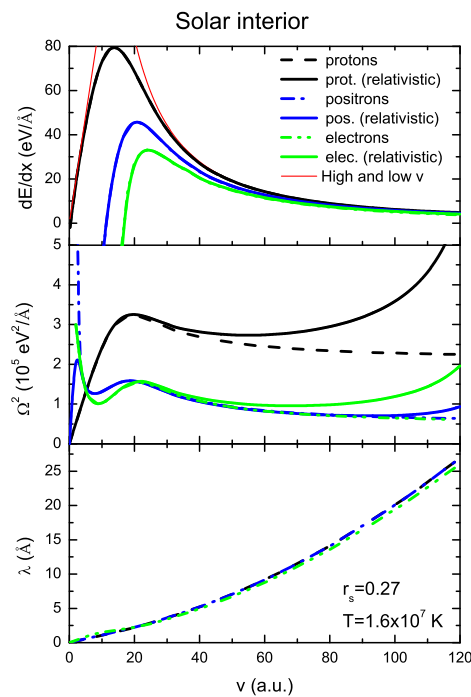

Figure 2. Energy loss moments of protons, positrons, and electrons traversing a solar interior electronic plasma.

Significant differences in the magnitude of the energy loss moments are appreciated when compared with the solar corona case. These differences are due to the great changes in densities and temperatures between both solar regions. Thus, for example, the results for the solar interior show a notorious increase in the stopping power values and a shift to larger velocities in the position of the stopping maximum. Here, two competing effects may be noticed: the increase in the density yields a significant increase in the maximum, while the increase in the temperature produces the opposite effect, i.e., a decrease in that maximum. In the competition between these effects, the first one is more relevant due to the fact that the density increases by several orders of magnitude; thus, the stopping power increases drastically compared with the values for the solar corona.

Finally, for this particular case, we find that the relativistic effects produce only small increments of the stopping values, negligible effects in the mean-free path for all particles, and very large effects in the straggling, particularly for protons. The explanation for these

differences stems from consideration of the contributions of close and distant collisions and from the additional influence of the so-called *density effect* in the energy loss of relativistic particles [50]. The treatment of these effects is described in Appendix A.

5.2. Giant Stars

Giant stars are important paradigms for studies of nuclear astrophysics and synthesis of elements. As early studies indicate, after the primordial hydrogen fuel is consumed, the star undergoes a series of fusion reactions of increasingly heavier elements [7–10]. At this stage, the core contracts by overwhelming gravitational forces, heating both the core and the surrounding material. The core then becomes hot enough to ignite new fusion reactions, starting with helium burning to form carbon, then burning carbon to form neon, oxygen, and silicon. Each of these reactions leads to an additional release of energy. One last cycle of fusion combines silicon nuclei to form iron. Considering, for example, the stages in the life of a $25 M_{sun}$ star, the times estimated for these processes range from about 500,000 years for He burning down to only 1 day for the final Si burning [9].

In the following, we show the results for different projectiles passing through different parts of the onion structure of a giant star, which take form once the series of fusion processes begins [10]. Going from outside to inside, we focus on the mantle composed of an He region, and a more internal O region, which comprises an external C sector and an internal Ne sector.

5.2.1. He Region

The intermediate He region of a giant star may be similar in density to the values already calculated for the solar interior; however, temperatures are much higher.

Figure 3 shows the results for typical values of density (2×10^2 g/cm^3) and temperature (2×10^8 K) in this region. The shift in the stopping curves already shown when passing from the external solar region to the solar interior is further observed here, together with a softening of the curve shapes as a result of the higher temperatures corresponding to this case. Some irregularity in the electron mean-free path for velocities below 60 a.u. is observed here, in the same region where the corresponding straggling curves also show a notorious change in shapes, and it may be shown that both effects have a common origin: the particular restrictions that apply to electrons. This behavior is analyzed and explained in Appendix B. The reason why this effect on the electron mean-free path was not observed in the previous figures is because the quantum restrictions for electrons become more relevant for higher temperatures.

Other interesting features found here are the magnitude of the relativistic effects observed in the straggling curves. These effects are in accord with those already found in Figure 2 and can be explained by the same reasons already mentioned; they are also described in Appendix A.

5.2.2. C + O Region

The composition of the following region of a giant star is dominated by completely ionized C and O atoms. The plasma electron density is estimated in the range of 10^3 g/cm^3, while temperatures range from 3 to 4×10^8 K.

Figure 4 shows the results for typical values of density (3×10^3 g/cm^3) and temperature (4×10^8 K) in this region.

Relativistic effects in the stopping curves are appreciated here due to the fact that the shift of the maximum approaches the relativistic range so the values are magnified. Also, large relativistic enhancements in the straggling curves are observed. The electron mean-free path curve shows also a larger enhancement and extends to larger velocities. As in the previous cases, no relativistic effects are observed in the mean-free path as a result of the density effect, and for the reasons explained in Appendix A.
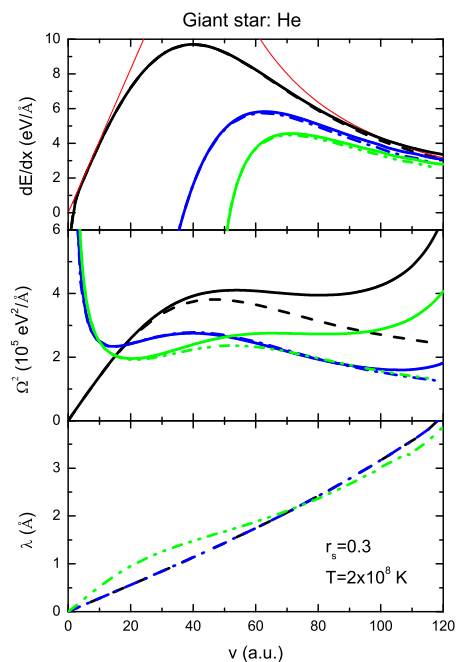
Figure 3. Energy loss moments of protons, positrons, and electrons traversing a giant star He region. Curves as in Figure 2.
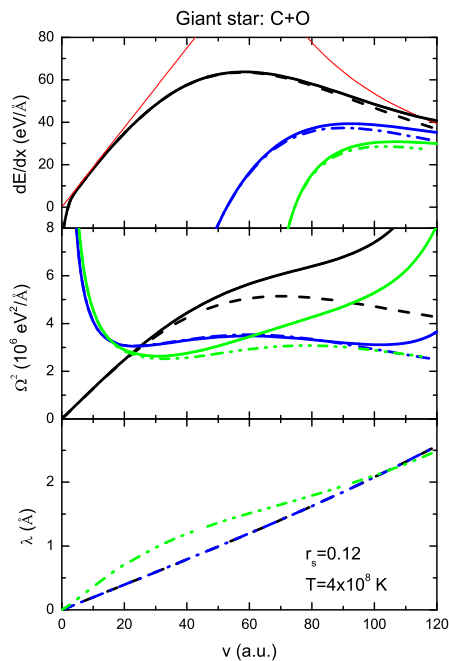

Figure 4. Energy loss moments of protons, positrons, and electrons traversing a giant star O-C region. Curves as in Figure 2.

5.2.3. Ne + O Region

The last case considered here, extending to still higher values of densities and temperatures, is the external sector of the Ne + O region. In this region, electron densities estimated by stellar structure models [10] are in the range of 10^4 to 10^6 g/cm^3, and temperatures are in the range of 10^8 to 10^9 K.

Figure 5 shows the results for a plasma with a density of 10^4 g/cm^3 and a temperature of 5×10^8 K. We notice similar behavior to that found in the previous regions, so that most

of the considerations made before also apply here. We notice an additional increase in all the effects already discussed due to the larger density and temperature values.

Finally, and although this study is concentrated in the set of three particles considered throughout this work, we wish to add here, only as an illustrative example, the case of muons, which may be considered as an intermediate case between heavy and light projectiles due to its mass ($m_\mu = 206.8$ a.u.). With this purpose, we included in Figure 5 a calculation of the stopping power for muons, shown by a grey line; the result is almost indistinguishable from the proton lines (both for the relativistic and non-relativistic calculations), except only at the low-velocity extreme, where we observe an anticipated drop to negative stopping values. Thus, and except for this minor effect, the energy-loss moments for muons are almost identical to those of equal velocity protons.
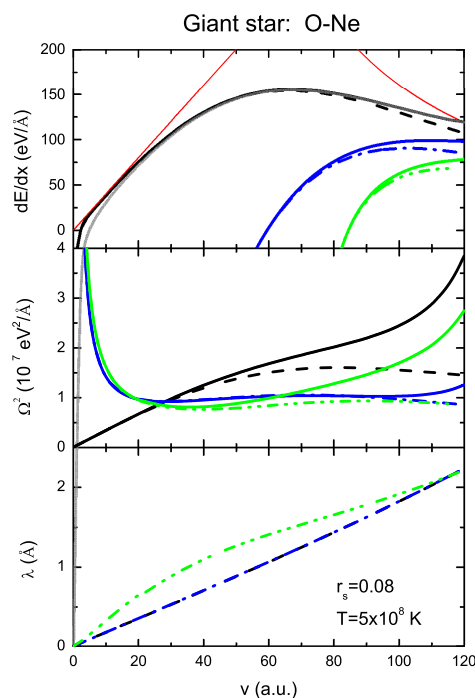

Figure 5. Energy loss moments of protons, positrons, and electrons traversing a giant star O-Ne region. The grey line (only distiguishable at very low *v*) shows the result for muons. The rest of the curves are as in Figure 2.

6. Summary and Conclusions

As stated in the Introduction, the interaction of energetic particles with stellar or interstellar plasmas spans an extremely wide area of interest for astrophysical studies. In this work, we have studied with detail those processes of interactions of charged subatomic particles with very hot plasmas in different stellar environments.

As described in this work, the study of these processes requires a combination of quantum and statistical aspects. Theoretical models that ignore some basic statistical properties, such as the effects of loss and gain processes in the energy exchange, cannot give correct results for the case of light particles as electrons and positrons, or for the straggling or mean-free path of heavy particles.

In previous works, we have developed a consistent method to describe these interactions within the framework of a quantum dielectric function approach together with a full account of the thermal and statistical aspects of the interactions. As shown here, the theoretical approach becomes particularly useful to describe processes occurring in various stellar interiors.

In the limit of high energies, relativistic corrections must be applied. However, these corrections attain different mathematical forms for each type of particle, and the corre-

sponding expressions are rather disperse in the literature since they were derived from different and more particular studies. Moreover, different corrections apply to close and distant interactions. Therefore, and for reasons of consistency, we reviewed the results obtained in those different sources for each of the particular cases and summarized the results in Appendix A. By integrating the basic expressions, we obtained the corrections to be applied for each particle and for each of the energy-loss moments.

One of the new and interesting questions is the difference between electrons and positrons, due to the special quantum restrictions that must be considered for electrons. This includes two types of restrictions arising from the identity between projectile and target electrons: quantum exchange effects, and the particular restriction in the maximum value of energy transfer in electron–electron collisions also arising from the particles' identity. The relevance of these restrictions and the effects on the energy exchange processes have been explained in Appendix B. Another important difference between light particles (electrons and positrons) and heavier ones (protons or other ions) is the recoil effect that imposes a much stricter limit on the maximum energy transfer in the case of light particles.

All these effects have been considered here in a consistent basis emerging from a general quantum statistical approach. The relevance of these effects, and the implications for interaction processes in stellar media, have been shown in a set of typical cases, going from dilute hot plasmas in the solar corona to progressively more dense media in stellar interiors.

The study includes the three relevant moments of the energy loss: the mean-free path, stopping power, and energy straggling, and each of the particles shows its own signature in the results.

As a general conclusion, we think the present work contributes to filling a gap in the knowledge of particle–plasma interactions that take place in many astrophysical environments and provides a consistent theoretical method, which is able to produce precise evaluations of the effects of all those interaction processes.

Appendix A. Relativistic Corrections

The parameter that characterizes the relativistic corrections to the energy loss of particles in matter is the term $(v/c)^2$. Hence, for particle speeds larger than about $c/2$ these corrections become significant.

The treatment of these corrections is different for protons, electrons, and positrons. In addition, the contributions from close and distant collisions are also quite different and must be treated separately.

In order to apply these corrections, we made a thorough review of treatments made by different authors, in particular those in Refs. [50–59]. The treatments, usually made for the stopping power, were extended to the calculations of mean free paths and straggling. For reasons of space and simplicity, we provide a brief summary of the different developments; a more complete description will be published elsewhere.

Appendix A.1. Treatment of Close Collisions

The analysis of close collisions starts from considerations of scattering cross sections of each type of incident particle with target electrons. For high energies of the incident particles, in the relativistic range, the target electrons may be assumed to be at rest.

The differential cross sections for protons, electrons, and positrons, given by the Mott [54], Möller [55], and Bhabha [56] formulas, respectively, in terms of the energy transfer W, are as follows:

$$\frac{d\sigma^{(Mott)}}{dW}\bigg|_{close} = \frac{A}{\beta^2 W^2}\left[1 - \beta^2\left(\frac{W}{W_{\max}}\right)\right] \tag{A1}$$

where

$$A = 2\pi Z^2 r_0^2 mc^2 = \frac{2\pi Z^2 e^4}{mc^2} \tag{A2}$$

where $r_0 = e^2/mc^2$ the classical electron radius, $W_{\max} = 2mv^2\gamma^2$ is the maximum energy transfer for proton–electron collisions, $\gamma = 1/\sqrt{1-\beta^2}$, and $\beta = v/c$,

$$\frac{d\sigma^{(Moller)}}{dW}\bigg|_{close} = \chi(v)\left[\frac{1}{W^2} + \frac{1}{(W - T(v))^2} + \left(\frac{\gamma - 1}{\gamma}\right)^2 \frac{1}{T(v)^2}\right.$$
$$\left. - \left(\frac{2\gamma - 1}{\gamma^2}\right)\frac{1}{W\,(T(v) - W)}\right] \tag{A3}$$

and

$$\frac{d\sigma^{(Bhabha)}}{dW}\bigg|_{close} = \chi(v)\left[\frac{1}{W^2} - \left(\frac{\gamma^2 - 1}{\gamma^2}\right)\frac{1}{W\,T(v)} + \frac{1}{2}\left(\frac{\gamma - 1}{\gamma}\right)^2\frac{1}{T(v)^2}\right.$$
$$\left. - \left(\frac{\gamma - 1}{\gamma + 1}\right)F_1(v, W) + \left(\frac{\gamma - 1}{\gamma + 1}\right)^2 F_2(v, W)\right] \tag{A4}$$

where $\chi(v) = 2\pi e^4/mv^2$, and $T(v) = (\gamma - 1)mc^2$ is the kinetic energy of the incident electron or positron.

The functions F_1 and F_2 are given by [53]

$$F_1(v, w) = \frac{1}{T(v)^2}\left[\left(\frac{\gamma + 2}{\gamma}\right)\frac{T(v)}{W} - 2\left(\frac{\gamma^2 - 1}{\gamma^2}\right) + \frac{W}{T(v)}\left(\frac{\gamma - 1}{\gamma}\right)^2\right] \tag{A5}$$

$$F_2(v, w) = \frac{1}{T(v)^2}\left[\frac{1}{2} + \frac{1}{\gamma} + \frac{3}{2\gamma^2} - \left(\frac{\gamma - 1}{\gamma}\right)^2\frac{W}{T(v)}\left(1 - \frac{W}{T(v)}\right)\right] \tag{A6}$$

Using these expressions, the stopping power due to close collisions is calculated as

$$S(v)|_{close} = n_e \int_{W_1}^{W_{\max}(v)} W\,\frac{d\sigma}{dW}\bigg|_{close}\,dW \tag{A7}$$

where n_e is the electron density, W_1 is an intermediate energy-transfer value, and $W_{\max}$ is the maximum energy transfer, given by $W_{\max} = 2mv^2\gamma^2$ for protons, $W_{\max} = T(v)$ for positrons, and $W_{\max} = T(v)/2$ for electrons (by the criterion of considering the new "primary" electron, the one with the largest outgoing energy after the collision).

In a similar way, the straggling and the inverse mean-free path may be calculated for the three types of particles replacing the factor W within the integral by W^2 and 1, respectively.

Appendix A.2. Treatment of Distant Collisions

Following Ref. [52], the differential cross section for momentum transfer in distant collisions may be written as

$$\frac{d\sigma}{dQ}\bigg|_{dist} = \frac{\chi(v)}{\hbar\overline{\omega}}\left[\frac{1}{Q} - \beta^2\frac{Q_{\min}(v)}{Q}\right] \tag{A8}$$

where $\overline{\omega}$ is a typical excitation frequency of the system (plasma frequency in our case), Q is a (quadratic) momentum transfer ($Q = |q^2|$ in the Berestetski's notation), and $Q_{\min}(v) = \overline{\omega}^2/(v\gamma)^2$.

As explained in [52,53], in the high-energy regime the differential cross section for distant interactions has the same form for all these particles.

Therefore, the contribution to the stopping power from distant collisions, with $Q_{min} < Q < Q_1$, is calculated by

$$S(v)|_{dist} = n_e \int_{Q_{\min}(v)}^{Q_1} \hbar\overline{\omega} \left.\frac{d\sigma}{dQ}\right|_{dist} dQ \tag{A9}$$

This integral can be calculated straightforwardly and yields

$$S(v)|_{dist} = n_e \chi(v) \left[\ln\left(\frac{Q_1}{Q_{\min}(v)}\right) - \beta^2 \right] = 2n_e \chi(v) \left[\ln\left(\frac{q_1 v\gamma}{\overline{\omega}}\right) - \frac{1}{2}\beta^2 \right] \tag{A10}$$

or in terms of the intermediate energy transfer W_1:

$$S(v)|_{dist} = n_e \chi(v) \left[\ln\left(\frac{2W_1}{\hbar^2 \omega_p^2} m v^2 \gamma^2\right) - \beta^2 \right] \tag{A11}$$

where we used the relation between the intermediate values of energy and momentum transfers

$$W_1 = \frac{\hbar^2}{2m} Q_1 = \frac{\hbar^2}{2m} q_1^2 \tag{A12}$$

This relation connects the intermediate values of the theories of Rohrlich and Carlson [53] and Berestetski et al. [52].

Appendix A.3. Density Effect

The results summarized before do not take into account the screening by plasma electrons, which is an important effect at large distances. Accounting for this effect gives rise to the so-called *density effect* in the energy loss.

The first theoretical description of this effect was made by Fermi [57], who obtained the density correction by integrating the flux of the Poynting vector through a cylindrical surface around the particle trajectory. The Fermi method was throroughly reviewed and discussed in a very clear way by Jackson [50].

A quantum mechanical study of the density effect was later made by Fano [58] and reviewed in detail by Ahlen [59]. The density correction is usually represented by a term $\delta/2$ that is subtracted from the logaritmic expression of the energy loss in the form [58,59]

$$S = \frac{4\pi n Z_1^2 e^4}{m v^2} \left[\ln\left(\frac{2mv^2}{I}\right) + \ln(\gamma^2) - \beta^2 - \frac{\delta}{2} \right] \tag{A13}$$

where I is the mean excitation energy [43], which is set equal to ω_p for a plasma [29,30], and δ is given by

$$\delta = \frac{2}{\pi \omega_p^2} \left[\int_0^\infty Im\left[\frac{-1}{\varepsilon(\omega)}\right] \ln\left[1 + \frac{\omega'^2}{\omega^2}\right] \omega \, d\omega - \frac{\pi}{2} \omega'^2 (1 - \beta^2) \right] \tag{A14}$$

The frequency ω' in this expression is given implicitly by the equation

$$\beta^2 \varepsilon(i\omega') = 1 \tag{A15}$$

While the solution of these equations may be a complicated task for solid targets when the details of the atomic structure are considered [60], it turns out that a rather simple solution may be obtained for the case of a plasma using the Drude expression

$$\varepsilon(\omega) = 1 - \frac{\omega_p^2}{\omega(\omega + i\delta)} \tag{A16}$$

with δ a positive infinitesimal.

This expression, although very simple, is quite appropriate to represent the long-range screening in a plasma [50].

Using this expression one obtains

$$\omega'^2 = \omega_p^2 \frac{\beta^2}{1 - \beta^2} \tag{A17}$$

and integrating Equation (A14), we obtain

$$\delta = \ln\left[\frac{1}{1 - \beta^2}\right] - \beta^2 = 2\left(\ln\gamma - \frac{1}{2}\beta^2\right) \tag{A18}$$

Replacing this in Equation (A13), we finally obtain

$$S = \frac{4\pi n Z_1^2 e^4}{mv^2}\left[\ln\left(\frac{2mv^2}{I}\right) + \ln\gamma - \frac{1}{2}\beta^2\right] \tag{A19}$$

By comparison with Equation (A13), we find that the significant effect of the density correction is to remove one of the γ factors in the $\ln(\gamma^2)$ term in Equation (A13).

This conclusion agrees with the analysis made by Jackson, who explains the origin of the density effect in terms of a cancellation of the relativistic increase in the range of the fields at large distances due to the screening of those fields by the plasma electrons. In this way, the net result is the removal of the γ factor associated with long-range interactions. To complete this analysis, we notice that the remaining $\ln(\gamma)$ term in Equation (A19) arises from the treatment of close collisions (i.e., maximum energy transfer in those collisions).

As is clear from this analysis (and from the Jackson discussions), the density correction in the relativistic range affects only the terms corresponding to distant interactions. For this reason, it is important in the calculations of stopping powers and mean free paths, but not for the energy straggling of relativistic particles, which is determined by close collisions.

Appendix B. Analisis of Gain and Loss Terms in the Energy Loss

The calculations illustrated in the various figures show some interesting differences in the results for the different particles. We want to explain here what the origin of these differences is.

For example, we refer here to the hump in the electron mean-free path observed in Figures 3–5. To explain this effect, we show in Figure A1 both the MFP (scale on the right of the figure) and inverse mean-free path (IMFP, scale on the left). Here, the line with squares shows the contribution of energy loss terms; the line with triangles is the contribution of energy gain terms, and the continuous line is the total IMFP.

The analysis of the IMFP gives a more direct insight because the contributions from gain and loss processes are additive in this case. The IMFP curves show very clearly what is the origin of this effect.

In the case of positrons, the contribution to the IMFP from loss and gain processes has the same type of divergent behavior (a $1/v$ dependence), and so in this case the MFP has a linear dependence on v for low velocities. On the other hand, the results for electrons show quite distinct behavior; the curve corresponding to energy gain processes has the same type of divergent behavior as for positrons, but the curve for loss processes has a maximum for intermediate values of v. This is the particular phenomenon that we wish to explain here.
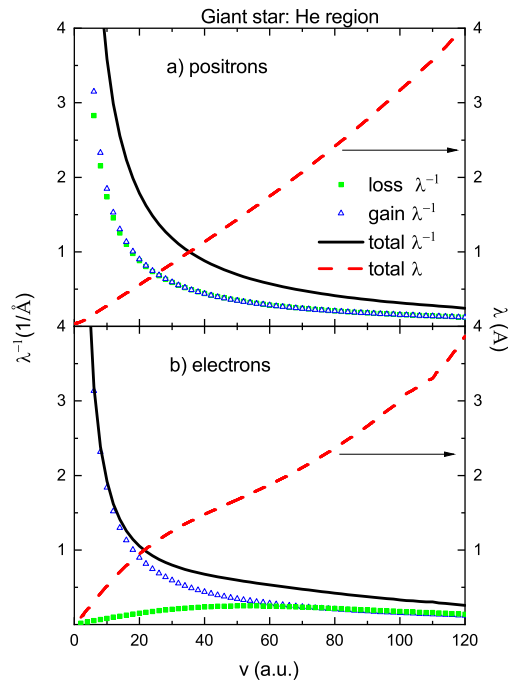
Figure A1. Gain and loss contributions to the inverse mean free path (left axis) and total mean free path (right axis) of (**a**) positrons and (**b**) electrons traversing a giant star He region.

The explanation stems from the quantum restrictions that apply to electrons, indicated as (i) and (ii) in the text after Equation (19). A detailed study of the effects produced by each of these restrictions indicates that the first one (exclusion principle) produces only a negligible effect (this is not surprising since in the present cases, where $k_B T >> E_F$, the occupation number of electron states is extremely low), so that the whole effect in the MFP is produced by the second restriction, i.e., the criterion that the electron that emerges with the largest energy after the interaction is to be considered as the new primary electron. We may also observe here that the restriction due to recoil effects, given by Equations (11) and (12), acts in the same way for electrons and positrons.

Hence, all the differences in the energy-loss moments for protons, positrons, and electrons are produced by the electron identity and the recoil effects. The action of the Bose factor serves to enhance these effects.

Appendix C. Low- and High-Energy Approximations

A well known analytical approximation for the stopping power of high-velocity particles was obtained by Bethe; the expression in the non-relativistic regime is the following

$$S_{high-v} = \frac{4\pi n Z^2 e^4}{mv^2} \ln\left(\frac{\alpha_1 m v^2}{\hbar \omega_p}\right), \tag{A20}$$

where Ze is the particle charge, and with $\alpha_1 = 2$ for protons, 1 for positrons, and $0.5\sqrt{e/2} = 0.583$ for electrons [43].

In the opposite limit, a low-velocity approximation that applies when $k_B T / E_F >> 1$ was obtained in Ref. [61], viz.

$$S_{low-v} \cong \frac{4}{3} \frac{(2\pi m)^{1/2}}{(k_B T)^{3/2}} Z^2 e^4 n v \left[\ln\left(\frac{k_B T}{\hbar \omega_p}\right) + \frac{1}{4}\right] \tag{A21}$$

These are the quantum-mechanical results. A similar expression, with the same forefactor but different logarithm, was obtained much earlier by Spitzer [15] for classical plasmas.

A still more general approximation that applies to plasmas with arbitrary degeneracy was also obtained in Ref. [61].

The ranges of applicability of Equations (A20) and (A21) are given by $v >> v_{th}$ and $v << v_{th}$ respectively, where $v_{th} = \sqrt{k_B T / m}$, and both are in excellent agreement with the results shown in Figures 1–5.

Notes

[1] Typical densities in white dwarfs are in the range of $10^4 - 10^7$ g/cm^3 while central densities may be as high as 10^8 g/cm^3; however, for densities beyond 10^6 g/cm^3 a relativistic model of dielectric response is required, including response to transverse fields not considered in this study. The relativistic corrections applied here refer to relativistic particles incident on non-relativistic plasmas. See refs. [1,12].

[2] The original derivation by Ochkur considers very high velocities and its function is written in terms of (q/v). However this function has an anomalous behavior when v approaches 0; therefore we find it convenient to introduce a velocity v', as a mean velocity for interactions between incident and plasma electrons. See ref. [36].

References

1. Hansen, C.J.; Kawaler, S.D.; Trimble, V. *Stellar Interiors: Physical Principles, Structure and Evolution*; Springer: New York, NY, USA, 2004.
2. Available online: www.sciencedirect.com/topics/physics-and-astronomy/interstellar-plasma (accessed on 6 August 2023).
3. Crammer, S.R.; Winebarger, A.R. The Properties of the Solar Corona and Its Connection to the Solar Wind. *Annu. Rev. Astron. Phys.* **2019**, *57*, 157. [CrossRef]
4. Di, L.; Sigalotti, G.; Cruz, F. Unveiling the mystery of solar-coronal heating. *Phys. Today* **2023**, *76*, 34.
5. Bethe, H.A. Energy production in stars. *Phys. Rev.* **1939**, *55*, 434. [CrossRef]
6. Bethe, H.A. Energy production in stars. *Am. Sci.* **1942**, *30*, 243.
7. Reeves, H. *Stellar Evolution and Nucleo-Synthesis*; Gordon and Breach: Philadelphia, PA, USA, 1968.
8. Clayton, D. *Principles of Stellar Evolution and Nucleosynthesis*; University of Chicago Press: Chicago, IL, USA, 1984.
9. Bethe, H.A.; Brown, G. How a Supernova explodes. *Sci. Am.* **1985**, *252*, 60. [CrossRef]
10. Arnett, W.D. Neutrino trapping during gravitational collapse of stars. *Astrophys. J.* **1977**, *218*, 815. [CrossRef]
11. Hayes, A.C.; Gooden, M.E.; Henry, E.; Jungman, G.; Wilhelmy, J.B.; Rundberg, R.S.; Yeamans, C.; Kyrala, G.; Cerjan, C.; Danielson, D.L.; et al. Plasma stopping-power measurements reveal transition from non-degenerate to degenerate plasmas. *Nat. Phys.* **2020**, *16*, 432–437. [CrossRef]
12. Chandrasekhar, S. The density of white-dwarf stars. *Philos. Mag.* **1931**, *7*, 592. [CrossRef]
13. Paxton, B.; Bildsten, L.; Dotter, A.; Herwig, F.; Lesaffre, P.; Timmes, F. Modules of Experiments in Stellar Astrophysics (MESA). *Astrophys. J. Suppl. Ser.* **2011**, *192*, 3. [CrossRef]
14. Gryzinski, M. Stopping Power of a Medium for Heavy, Charged Particles. *Phys. Rev.* **1957**, *107*, 1471. [CrossRef]
15. Spitzer, L. *Physics of Fully Ionized Gases*; Interscience: New York, NY, USA, 1962.
16. Butler, S.T.; Buckingham, M.J. Energy Loss of a Fast Ion in a Plasma. *Phys. Rev.* **1962**, *126*, 1. [CrossRef]
17. de Ferrariis, L.; Arista, N.R. Classical and quantum mechanical treatments of the energy loss of charged particles in dilute plasmas. *Phys. Rev. A* **1984**, *29*, 2145. [CrossRef]
18. Pines, D.; Bohm, D. Collective vs Individual Particle Aspects of the Interactions. *Phys. Rev.* **1952**, *85*, 338. [CrossRef]
19. Kihara, T.; Aono, O. Unified theory of relaxations in plasmas. *J. Phys. Soc. Jpn.* **1963**, *18*, 837. [CrossRef]
20. Peter, T.; Meyer-ter-Vehn, J. Energy loss of heavy ions in dense plasma. Linear and nonlinear Vlasov theory for the stopping power. *Phys. Rev. A* **1991**, *43*, 1998. [CrossRef] [PubMed]
21. Archubi, C.D.; Arista, N.R. Unified description of interactions and energy loss of particles in dense matter and plasmas. *Phys. Rev. A* **2020**, *102*, 052811. [CrossRef]
22. Archubi, C.D.; Arista, N.R. General formulation of interactions and energy loss of particles in plasmas: Quantum-wave-packet model versus a semiclassical approach. *Phys. Rev. A* **2022**, *105*, 032806. [CrossRef]
23. Platzman, P.M.; Wolff, P.A. *Elementary Excitations in Solid-State Plasmas*; Academic Press: New York, NY, USA, 1973.
24. Arista, N.R.; Brandt, W. Energy loss and straggling of charged particles in plasmas of all degeneracies. *Phys. Rev. A* **1981**, *23*, 1898. [CrossRef]
25. Kaneko, T. Wave packet theory of bound electrons. *Phys. Rev. A* **1989**, *40*, 2188. [CrossRef]
26. Kaneko, T. Partial and Total Electronic Stoppings of Solids and Atoms for Energetic Ions. *Phys. Stat. Sol.* **1989**, *156*, 49. [CrossRef]
27. Kaneko, T. Partial and total electronic stopping cross sections of atoms and solids for protons. *At. Data Nucl. Data Tables* **1993**, *53*, 271. [CrossRef]
28. Inokuti, M. Inelastic Collisions of Fast Charged Particles with Atoms and Molecules—The Bethe Theory Revisited. *Rev. Mod. Phys.* **1971**, *43*, 297. [CrossRef]
29. Lindhard, J. On the properties of a gas of charged particles. *Mat. Fys. Medd. Dan. Vid. Selsk* **1954**, *28*, 1–57.
30. Lindhard, J.; Winther, A. Stopping power of electron gas and equipartition rule. *Mat. Fys. Medd. Dan. Vid. Selsk* **1964**, *34*, 1–22.

31. Ritchie, R.H. Interaction of charged particles with a degenerate Fermi–Dirac electron gas. *Phys. Rev.* **1959**, *114*, 644. [CrossRef]
32. Arista, N.R.; Brandt, W. Dielectric response of quantum plasmas in thermal equilibrium. *Phys. Rev. A* **1984**, *29*, 1471. [CrossRef]
33. Bringa, E.M.; Arista, N.R. Energy loss of correlated ions in plasmas: Collective and individual contributions. *Phys. Rev. E* **1996**, *54*, 4101. [CrossRef] [PubMed]
34. Pines, D. Classical and Quantum Plasmas. *Plasma Phys.* **1961**, *2*, 5. [CrossRef]
35. Sitenko, A.G. *Electromagnetic Fluctuations in Plasma*; Academic Press: New York, NY, USA, 1967.
36. Ochkur, V.I. Ionization of the Hydrogen Atom by Electron Impact With Allowance for the Exchange. *Soviet Phys. JETP* **1964**, *47*, 1766.
37. Bransden, B.H. Atomic Collision Theory. In *Lecture Notes and Supplements in Physics, Mathematics Lecture Note Series*; Benjamin, W.A., Ed.; Benjamin Cumming: San Francisco, CA, USA, 1970; Volume 12, ISSN 1053-9824.
38. Fernández-Varea, J.M.; Mayol, R.; Liljequist, D.; Salvat, F. Inelastic scattering of electrons in solids from a generalized oscillator strength model using optical and photoelectric data. *J. Phys. Condens. Matter* **1993**, *5*, 3593. [CrossRef]
39. García-Molina, R.; Abril, I.; Kyriakou, I.; Emfietzoglou, D. Inelastic scattering and energy loss of swift electron beams in biologically relevant materials. *Surf. Interface Anal.* **2017**, *49*, 11. [CrossRef]
40. de Vera, P.; García-Molina, R. Electron inelastic mean free paths in condensed matter down to a few electronvolts. *J. Phys. Chem. C* **2019**, *123*, 2075. [CrossRef]
41. Hippler, R.; Jitschin, W. Plane Wave Born Cross Sections Including Exchange for K-Shell Ionization of Light Atoms. *Z. Phys. A Atoms Nucl.* **1982**, *307*, 287–292. [CrossRef]
42. Shinotsuka, H.; Tanuma, S.; Powell, C.J.; Penn, D.R. Calculations of Electron Stopping Power for 41 Elemental Solids Over the 50 eV to 30 keV Range With the Full Penn Algorithm. *Nucl. Instrum. Methods Phys. Res. B* **2012**, *270*, 75–92. [CrossRef]
43. Bethe, H.A.; Ashkin, J. Passage of Radiation through matter. In *Experimental Nuclear Physics*; Segré, E., Ed.; Wiley: New York, NY, USA, 1953.
44. Archubi, C.D.; Arista, N.R. A comparative study of threshold effects in the energy loss moments of protons, electrons, and positrons using dielectric models for band gap materials. *Eur. Phys. J. B* **2017**, *90*, 18. [CrossRef]
45. Schmeltz, J.T.; Reames, D.V.; Von Steiger, R.; Basu, S. Composition of the Solar Corona, Solar Wind, and solar Energetic Particles. *Astrophys. J.* **2012**, *755*, 33. [CrossRef]
46. Barriga-Carrasco, M.D.; Chacón-Rubio, F.; Montanari, C.C. Stopping power of plasma free and bound electrons using dielectric formalism. *Eur. Phys. J. Plus* **2022**, *137*, 375. [CrossRef]
47. Archubi, C.D.; Montanari, C.C.; Arista, N.R. Dielectric approaches for interactions of protons, positrons, and electrons in cold matter and plasmas. *Phys. Rev. A* **2023**, *108*, 012822. [CrossRef]
48. Warren, H.P.; Brooks, D.H. The Temperature and Density Structure of the Solar Corona. Observations of the Quiet Sun With the EUV Imaging Spectrometer on Hinode. *Astrophys. J.* **2009**, *700*, 762. [CrossRef]
49. Dudík, J.; Del Zanna, G.; Rybák, J.; Lörinčík, J.; Dzifčáková, E; Mason, H.E.; Tomczyk, S.; Galloy, M. Electron Densities in the Solar Corona Measured Simultaneously in the Extreme Ultraviolet and Infrared. *Astrophys. J.* **2021**, *906*, 118. [CrossRef]
50. Jackson, J.D. *Classical Electrodynamics*, 2nd ed.; John Wiley and Sons: New York, NY, USA, 1975.
51. Eby, P.B.; Morgan, S.H. Charge Dependence of Ionization Energy Loss for Relativistic Heavy Nuclei. *Phys. Rev. A* **1972**, *5*, 2536. [CrossRef]
52. Berestetskii, V.B.; Lifshitz, E.M.; Pitaevskii, L.P. *Quantum Electrodynamics*; Pergamon Press: Oxford, UK, 1982.
53. Rohrlich, F.; Carlson, B.C. Positron-Electron Differences in Energy Loss and Multiple Scattering. *Phys. Rev.* **1954**, *91*, 38. [CrossRef]
54. Mott, N.F. On the Theory of Excitation by Collision with Heavy Particles. *Proc. Camb. Phil. Soc.* **1931**, *27*, 553. [CrossRef]
55. Moller, C. Zur Theorie des Durchgangs shneller Elektronen Durch Materie. *Ann. Phys.* **1932**, *14*, 531. [CrossRef]
56. Bhabha, H.J. The scattering of positrons by electrons with exchange on Dirac's theory of the positron. *Proc. R. Soc. Lond.* **1936**, *A154*, 195.
57. Fermi, E. The Ionization Loss of Energy in Gases and in Condensed Materials. *Phys. Rev.* **1940**, *57*, 485. [CrossRef]
58. Fano, U. Penetration of protons, alpha particles, and mesons. *Ann. Rev. Nucl. Sci.* **1963**, *13*, 1–66. [CrossRef]
59. Ahlen, S.P. Theoretical and experimental aspects of the energy loss of relativistic heavily ionizing particles. *Rev. Mod. Phys.* **1980**, *52*, 121. [CrossRef]
60. Sternheimer, R.M. The Density Effect for the Ionization Loss in Various Materials. *Phys. Rev.* **1952**, *88*, 851. [CrossRef]
61. Arista, N.R. Low-velocity stopping power of semi-degenerate quantum plasmas. *J. Phys. C Solid State Phys.* **1985**, *18*, 5127. [CrossRef]